Inhibitors of trehalose-6-phosphate synthase activity in fungal pathogens compromise thermal tolerance pathways

Yi Miao[a*1], Vikas Yadav[b1], William Shadrick[c^], Jiuyu Liu[c], Alexander R. Jenner[c], Connie B. Nichols[bd], Clifford Gee[c@], Martin Schäfer[a%], Jennifer L. Tenor[d], John R. Perfect[b,d], Richard E. Lee[c], Richard G. Brennan[a#], and Erica J. Washington[a,b#]

[a]Department of Biochemistry, Duke University School of Medicine, Durham, North Carolina, USA

[b]Department of Molecular Genetics and Microbiology, Duke University School of Medicine, Durham, North Carolina, USA

[c]Department of Chemical Biology and Therapeutics, St. Jude Children's Research Hospital, Memphis, Tennessee, USA

[d]Division of Infectious Diseases, Department of Medicine, Duke University School of Medicine, Durham, North Carolina, USA

#Address correspondence to: erica.washington1@duke.edu and richard.brennan@duke.edu

*Present address: Division of Life Science, The Hong Kong University of Science and Technology, Clear Water Bay, Kowloon, Hong Kong SAR, China

^Present address: Incyte Corporation, Wilmington, Delaware

@Present address: Department of Chemistry and Biochemistry, Creighton University, Omaha, Nebraska, USA

%Present address: GCP-Service International Ltd & Co. KG, Bremen, Germany

[1] co-first authors

Running title

Inhibition of fungal trehalose biosynthesis

Keywords: trehalose, Tps1, *Cryptococcus*, *Candida*, antifungal

Abstract

Infections caused by fungal pathogens such as *Candida* and *Cryptococcus* are associated with high mortality rates, partly due to limitations in the current antifungal arsenal. This highlights the need for antifungal drug targets with novel mechanisms of action. The trehalose biosynthesis pathway is a promising antifungal drug target because trehalose biosynthesis is essential for virulence in *Cryptococcus neoformans* and *Candida albicans* and is also a mediator of fungal stress responses, such as thermotolerance. To exploit its untapped antifungal potentials, we screened the St. Jude 3-point pharmacophore library to identify small molecule inhibitors of the first enzyme in the trehalose biosynthesis pathway, trehalose-6-phosphate synthase (Tps1). Structure-guided optimization of a potent hit, SJ6675, yielded a water-soluble inhibitor named 4456dh. Employing biochemical, structural and cell-based assays, we demonstrate that 4456dh inhibits Tps1 enzymatic activity, suppresses trehalose synthesis and exerts a fungicidal effect. Notably, the structure of Tps1 in complex with 4456 reveals that 4456 occupies the substrate binding pocket. Importantly, 4456dh renders normally thermotolerant fungal pathogens unable to survive at elevated temperatures, which is critical as we investigate the emergence of fungi from the environment due to a warming climate. Overall, this work develops the water-soluble 4456dh as an early-stage antifungal drug that has a distinct mechanism of action compared to existing clinical antifungals.

50 **Importance**

51 The rise of fungal infections in recent years is alarming due to an increase in the vulnerable
52 immunocompromised population, global temperature increase and limited antifungal treatment
53 options. One of the major hurdles in developing new drugs is the identification of fungal-specific
54 antifungal drug targets due to highly conserved cellular machinery between fungi and humans.
55 Here, we describe a small molecule inhibitor, 4456dh, of the trehalose biosynthesis pathway. This
56 pathway is present in fungi but not humans. Trehalose plays a critical role in stress responses
57 such as thermotolerance in fungal pathogens and is essential for their virulence. We show that
58 treatment with 4456dh blocks production of trehalose and renders fungal cells inviable. Thus far,
59 4456dh is active against two fungal pathogens of critical importance suggesting a broad-spectrum
60 activity.

61 **Introduction**

62 The contribution of fungal pathogens to human mortality goes greatly unnoticed compared
63 to that of viruses and bacteria and even other eukaryotic pathogens. Remarkably, the combined
64 mortality associated with fungal pathogens is similar to that caused by malaria and tuberculosis
65 (1). Each year a diverse collection of fungal pathogens cause diseases that result in
66 approximately 6.5 million infections and 2.5 million directly attributable deaths worldwide (2). The
67 World Health Organization recently documented the significance of these fungal pathogens and
68 listed *Cryptococcus neoformans* and *Candida albicans* as critical pathogens, amongst others, and
69 made the call for increased development of antifungal therapeutics, fungal surveillance and
70 diagnostics (3).

71 The current antifungal drug armamentarium consists of polyenes, azoles and
72 echinocandins. While these antifungal drugs have proven to be powerful, they also have
73 drawbacks that include the lack of bioavailability, lack of effectiveness against multiple pathogens
74 and an increase in the likelihood of antifungal drug resistance (4). Current antifungal drugs are
75 also often toxic and require long and difficult treatment regimens (5). Therefore, these drugs are
76 insufficient to control the current state of fungal infections. Moreover, new fungal pathogens, such
77 as the multidrug-resistant thermotolerant yeast *Candida auris*, are emerging due to a warming
78 climate (6–11).

79 Because fungi and humans are both eukaryotes, it is difficult yet advantageous to identify
80 an antifungal drug target that is not conserved between both species. An antifungal drug with a
81 target not found in humans is likely to have fewer off-target effects and be less toxic for the
82 immunocompromised patients who are susceptible to invasive fungal infections. Other features
83 of antifungal drugs that are desirable include the possibility of being broad-spectrum in the case
84 of poor diagnostics and a low likelihood that resistance to the antifungal drug will develop.

85 The trehalose biosynthesis pathway in fungal pathogens has been described as a
86 promising antifungal drug target (12). The trehalose biosynthesis pathway is conserved amongst

87 insects, plants, bacteria and fungi (13). However, the trehalose biosynthesis pathway is not found
88 in mammals (12, 13). Given that the key components of the trehalose biosynthesis pathway are
89 structurally conserved, it may be possible to generate a broad-spectrum antifungal drug that
90 targets its components. Attempts have been made to generate compounds that inhibit trehalose
91 biosynthesis in insects (14). Closantel was identified as a potential bioactive molecule that targets
92 the trehalose biosynthesis pathway and has potent activity against *C. neoformans* and
93 *Cryptococcus gattii in vitro*. However, closantel does not have antifungal activity in murine models
94 (12).

95 The trehalose biosynthesis pathway in fungal pathogens is a two-step process initiated
96 when trehalose-6-phosphate synthase, Tps1, converts uridine-diphosphate-glucose (UDPG) and
97 glucose-6-phosphate (G6P) to trehalose-6-phosphate (T6P) (15). T6P is dephosphorylated by the
98 trehalose-6-phosphate phosphatase (Tps2) to produce trehalose (15). Several pathogens also
99 contain additional trehalose biosynthesis proteins. For example, in *Aspergillus fumigatus* there
100 are apparently multiple Tps1 enzymes (16). In ascomycetes, including *A. fumigatus*, *C. albicans*
101 and *S. cerevisiae,* there are regulatory trehalose biosynthesis proteins, which lack catalytic activity
102 and are thought to act as scaffolds to enable complex formation of the trehalose biosynthesis
103 proteins (17).

104 Trehalose is a nonreducing disaccharide composed of two glucose molecules linked by
105 an α,α-1,1-glycosidic bond (α-D-glucopyranosyl-(1→1)-α-D-glucopyranoside). Trehalose is a
106 highly stable molecule that can help proteins and cellular membranes withstand dehydration,
107 salinity, and heat (18–20). Trehalose can also serve as an energy source and is broken down by
108 trehalase into two glucose molecules that funnel into energy-generating pathways such as
109 glycolysis and the pentose phosphate pathway (15, 21, 22). Importantly, the trehalose
110 biosynthesis pathway is strongly associated with virulence in *C. neoformans* and *C. albicans*. In
111 the absence of *TPS1* and *TPS2*, *Cryptococcus* and *Candida* species cannot survive in
112 mammalian hosts (23–27). The contribution of trehalose biosynthesis to thermotolerance in *C.*

113 *albicans* and *C. neoformans* is critical. The inhibition of trehalose biosynthesis may help control
114 the expansion of thermotolerant environmental isolates, which have the potential to become
115 pathogens.

116 We now have the tools to take a structure-based approach to developing an inhibitor of
117 Tps1. The recent determination of structures of trehalose biosynthesis proteins from fungal
118 pathogens, including *C. albicans* and *A. fumigatus* has enabled us to utilize a structure-guided
119 approach to designing inhibitors of trehalose biosynthesis proteins (28, 29). Most recently, cryo-
120 electron microscopy was used to determine detailed binding residues in the *C. neoformans*
121 substrate-binding pocket (30). Tps1 is a GT-B family, retaining glycosyltransferase and contains
122 two catalytic subdomains, connected by a kinked, C-terminal α-helix (31). The N-terminal
123 subdomain binds the sugar acceptor, G6P, and the C-terminal subdomain contains the donor,
124 UDPG. Given that Tps1 utilizes a substrate-assisted mechanism of catalysis, proper alignment of
125 each substrate is required for the formation of T6P. Therefore, targeting the substrate-binding
126 pocket is a critical and facile route to disrupt the function of Tps1. Additionally, the ability to
127 generate large amounts of pure recombinant *C. neoformans* Tps1 and *C. albicans* Tps1
128 expressed and purified in *E. coli* has made high-throughput compound screens possible.

129 In this work, we developed a fluorescence polarization-based high-throughput screening
130 platform and screened a chemical library containing 750 compounds to identify Tps1 inhibitors.
131 We determined the structure of a top hit bound to *C. albicans* Tps1. Guided by this structural
132 information, we rationally optimized the hit and developed a water-soluble derivative, 4456dh.
133 4456dh demonstrates broad-spectrum inhibitory effects against multiple pathogenic fungal
134 species, including *Candida* and *Cryptococcus*. Furthermore, 4456dh displays temperature-
135 dependent fungicidal activity, phenocopying the *tps1*Δ fungicidal phenotype. Finally, we show that
136 in fungal cells 4456dh inhibits the biosynthesis of trehalose. These data indicate that the
137 mechanism of action of 4456dh is indeed trehalose-dependent and fully exploits the "druggable"
138 thermotolerant characteristics of various pathogenic fungal species.

Overall, this work highlights the combination of high-throughput screening, structure-guided hit optimization and cellular assays to develop a promising water-soluble small molecule with desired antifungal properties and the potential for development of a new antifungal therapeutic.

144 **Results**

145 **Seven compounds were identified from a high-throughput screen to inhibit CaTps1 activity**

146 As the first step of the trehalose biosynthesis pathway, Tps1 synthesizes T6P from the
147 substrates UDP-glucose and G6P followed by the release of UDP and T6P (15). To identify a
148 small molecule inhibitor of Tps1 activity, we adapted a high-throughput screen (HTS) utilizing the
149 UDP Transcreener Fluorescence Polarization (FP) assay (32, 33). The FP assay detects the UDP
150 released as a result of the Tps1-mediated enzymatic reaction (Fig. 1A). The FP assay Z' factor,
151 which describes the suitability of an assay for a HTS, is 0.87, indicating an ideal signal-to-noise
152 ratio (Fig. S1A) (34). There was a greater than 175 millipolarization (mP) shift between the positive
153 control novobiocin, an inhibitor with activity against a bacterial trehalose-P-synthase, and the
154 negative control DMSO (Fig. S1A) (35). Recombinant Tps1 from *C. albicans*, hereafter referred
155 to as CaTps1, was expressed in *E. coli* and purified via an N-terminal 6xHis-tag and Ni^{2+}-NTA
156 affinity chromatography, followed by size exclusion chromatography (Fig. 1B). A 3-point
157 pharmacophore (3PP) library, which consisted of a subset of 750 compounds of less than 300 Da
158 in molecular mass from the St. Jude Children's Research Hospital chemical library, was screened
159 for the ability to inhibit 6xHis-CaTps1 activity (36). In the primary screen, 32 (4.3 %) compounds
160 that inhibited the activity of 6xHis-CaTps1 by more than 10% at 500 μM concentration were
161 identified (Fig. 1C,D). A 10% cutoff provided significant number of hits to validate using a dose
162 response assay (Fig. S1B). At the completion of the screen, seven compounds that inhibit the
163 activity of CaTps1 in a dose-dependent manner were selected for further investigation (Fig. 1E
164 and Table 1).

165 **Generation of a library of derivatives of SJ6675**

166 We initiated a structure-guided approach to generate derivatives of the compounds by
167 attempting *de novo* co-crystallization of each of the seven compounds with CaTps1. We
168 successfully obtained a 3.5 Å resolution structure of SJ6675 ((4-furan-3-yl)thiazol-2-amine) in
169 complex with CaTps1 (Fig. S2A and Table S1). This structure revealed the presence of SJ6675

170 in the substrate-binding pocket of CaTps1 (Fig. S2A), proximal to conserved substrate-binding
171 residues R280, K285, N382 and L383 (28). These data indicate that SJ6675 likely interferes
172 competitively with the binding of the UDPG substrate.

173 We designed a library of SJ6675 derivatives and tested the derivatives for inhibition of
174 CaTps1 activity (Fig. S2B,C). Many of the compounds, diluted in DMSO, precipitated when added
175 to the Tps1 activity assay reaction and several of the compounds increased the activity of CaTps1
176 (Fig. S2C). However, one of these compounds, 4456, significantly inhibited the activity of CaTps1
177 and did not precipitate in the assay solution (Fig. S2C).

178 **4456dh binds Tps1 with high affinity and inhibits the Tps1-mediated release of UDP**

179 To determine the ability to use 4456 as a lead compound using biochemical approaches,
180 we generated a water-soluble derivative of 4456, which we shall now refer to as 4456dh, for 4456-
181 dichloride hydrate (Fig. 2A). The composition of 4456dh was confirmed by NMR and elemental
182 analysis (Fig. S3).

183 Thermal shift assays were completed to determine if 4456dh binds Tps1. We
184 hypothesized that the binding of 4456dh to Tps1 would increase Tps1 stability, resulting in a
185 higher melting temperature. Therefore, CaTps1 and *C. neoformans* Tps1, hereafter referred to as
186 CnTps1, were incubated with 4456dh overnight at 4 °C. Glo-Melt dye was added to the mixture
187 prior to determining the thermostability. Surprisingly, we observed that 4456dh decreased the
188 melting temperature of both CaTps1 and CnTps1 in thermal shift assays indicating a
189 destabilization of the Tps1 enzyme upon binding (Fig. 2B,C). These data indicate that 4456dh
190 binds to both CaTps1 and CnTps1 but leads to destabilization of the Tps1 enzyme.

191 To determine the binding affinity of 4456dh and CaTps1 and CnTps1, microscale
192 thermophoresis (MST) was used. Given the intrinsic fluorescence of CaTps1 and CnTps1, we
193 were able to detect binding without the use of additional fluorophores. MST experiments revealed
194 that the binding affinities of 4456dh with recombinant 6xHis-CaTps1 and 6xHis-CnTps1 are 7.1

195 μM and 33.4 μM, respectively (Fig. 2D,E). These binding affinities are consistent with the
196 concentration of 4456dh at which we can detect a shift in Tps1 stability in the thermal shift assays.
197 The ability of 4456dh to inhibit the activity of CaTps1 was tested using a
198 spectrophotometric-coupled Tps1 enzyme assay, in which recombinant 6xHis-CaTps1 was
199 incubated with 1 mM 4456dh at 4 °C for 16 hours. The activity of 6xHis-CaTps1 was reduced
200 approximately 30% in the presence of 4456dh (Fig. 2F). Similarly, the effect of 1 mM 4456dh on
201 6xHis-CnTps1 activity was determined. 4456dh inhibited the activity of 6xHis-CnTps1 activity by
202 approximately 30% (Fig. 2G). Therefore, 4456dh directly binds and inhibits the activity of Tps1
203 from *C. albicans* and *C. neoformans*.

204 **4456dh binds the substrate-binding pocket of CaTps1**

205 To gain insight into the mode of action of 4456dh, we grew crystals of 6xHis-tagged *C.*
206 *albicans* Tps1 (6xHis-CaTps1) in complex with 4456 and determined the structure to a moderate
207 3.35 Å resolution (Fig. 3A and Table 2). The structure of the 6xHis-CaTps1-4456 complex was
208 solved using molecular replacement and the structure of CaTps1 bound to UDP and G6P (PDB:
209 5HUU), with UDP and G6P removed as the search query. The final model of the 6xHis-CaTps1-
210 4456 complex consists of N-terminal and C-terminal subdomains comprising residues 6 to 239
211 and 246 to 437, respectively, followed by the C-terminal α-helix (Fig. 3A). The final model also
212 contains one 4456 molecule per subunit of 6xHis-CaTps1 (Fig. 3A,B).
213 During refinement, electron density corresponding to 4456 was identified in the substrate-
214 binding pocket of CaTps1 between the N-terminal G6P-binding lobe and the C-terminal UDPG-
215 binding lobe. Polder omit maps, which exclude bulk solvent to allow for detection of weak density,
216 of the bound inhibitor reveal the binding of 4456 (Fig. S4) (37). 4456 was modelled into the
217 electron density between these two lobes and was found to make contacts with multiple
218 conserved residues and functionally critical substrate-binding residues (Fig. 3C and Fig. S5) (28).
219 The conserved residues near 4456 (Y89, R280, P316, S317, R318 and N382) are proximal to the
220 native product, UDP, and substrate G6P (Fig. 3D) that are required for catalytic activity. For

221 example, the hydroxyl group of the side chain of Y89 makes hydrophilic interactions with the G6P
222 phosphate moiety and mutation of Y89 to phenylalanine results the elimination of Tps1 activity
223 (28). The model of the catalytic modified-Rossman fold domains and the C-terminal α-helix is
224 structurally similar to previously determined structures of Tps1 from *C. neoformans*, *A. fumigatus*
225 and *E. coli,* and therefore, demonstrate the likelihood that 4456 also binds in the conserved
226 catalytic pockets of Tps1 from these additional organisms (Fig. S6A) (28, 30). Using a ConSurf
227 analysis, the degree of conservation was mapped onto Tps1 structures and revealed that the
228 most highly conserved residues are either buried in the substrate-binding pocket or are proximal
229 to that region (Fig. S6B) (38). This finding was expected given that 4456 is a derivative of a lead
230 compound that also binds the substrate-binding pocket of CaTps1 (Fig. S2).

231 **4456dh is bioactive against *Candida* and *Cryptococcus* cells**

232 We tested the effects of 4456dh on live cells by determining the minimal inhibitory
233 concentration causing 80% growth reduction (MIC_{80}). Wild-type *C. albicans* and *C. auris* cells
234 were incubated with 4456dh in yeast-peptone-dextrose (YPD) medium at 42 °C and 39 °C,
235 respectively (Fig. 4A). 4456dh inhibited the growth of *C. albicans* at 42 °C with an MIC_{80} of 13
236 mM, whereas no MIC was detected at 30 °C (Figure 4A and Fig. S7A). 4456dh inhibited the
237 growth of *C. auris* with an MIC_{80} of 7 mM at 39 °C (Fig. 4A). The MIC_{80} increased at 30 °C to
238 greater than 13 mM (Fig. S7A). We characterized the fungicidal activity of 4456dh by growing the
239 *C. albicans* on compound-free YPD plates after exposure to 4456dh and observed temperature-
240 dependent fungicidal activity of 4456dh on *C. albicans* at 42 °C (Fig. 4A and Fig. S7B).
241 Interestingly, fungicidal activity of 4456dh on *C. auris* was also detected at both 30 °C and 39 °C
242 (Fig. 4A and Fig. S7B).

243 4456dh displayed the most potent activity on *C. glabrata*, with an MIC_{80} of 7.8 μM at 42
244 °C (Fig. 4B). Furthermore, there was significant fungicidal activity of 4456dh on *C. glabrata* in
245 concentrations starting at approximately 7.8 μM (Fig. 4B). The activity against *C. glabrata* was
246 specific to 42 °C, as no MIC or fungicidal activity was detected at 30 °C (Fig. S7A,B).

247 We next tested the activity of 4456dh on *Cryptococcus* species at 37 °C. We found that
248 4456dh inhibited the growth of *C. neoformans*, *C. deneoformans*, and *C. gattii* with MIC_{80} of 7
249 mM, 3 mM, and 7 mM, respectively (Fig. 4C). Fungicidal activity of 4456dh was also detected in
250 all the *Cryptococcus* species tested at 37 °C (Fig. 4C). Interestingly, 4456dh also displayed
251 fungicidal activity on *C. deneoformans* at 30 °C at 13 mM (Fig. S7C).

252 Given that *C. neoformans tps1*Δ yeasts are fungicidal at elevated temperature and not at
253 30 °C, the fungicidal activity of 4456dh at 30 °C indicated that in addition to Tps1 there is another
254 target of 4456dh. To test this hypothesis, we performed zone of inhibition studies in the *C.*
255 *deneoformans* background (Fig. S8A). At 37 °C, there was a distinct zone of inhibition surrounding
256 4456dh (Fig. S8A). Consistent with our prediction of an additional target of 4456dh, we detected
257 a diffuse, yet visible zone of inhibition due to 4456dh on *C. deneoformans tps1*Δ cells (Fig. S8B).

258 Inhibitors of Tps1 may work synergistically with known antifungal drugs. In *C. glabrata* the
259 trehalose biosynthesis mutant, *tps2*Δ, is more susceptible to fluconazole at 37 °C (39). Therefore,
260 we hypothesized that there might be synergy between 4456dh and fluconazole. We performed
261 Epsilometer tests (E-tests) and detected synergy between 4456dh and fluconazole in *C.*
262 *neoformans H99* in a dose-dependent manner (Fig. S9).

263 **4456dh inhibition mimics loss of functional Tps1**

264 Given that 4456dh inhibits the activity of CaTps1 and CnTps1 *in vitro* and has bioactivity
265 against multiple *Candida* and *Cryptococcus* species, we tested if 4456dh affects trehalose
266 production in cells. We quantified trehalose levels in cells treated with 4456dh at sub-lethal
267 concentrations as determined by the MIC assays using a colorimetric spectrophotometric assay.
268 We measured trehalose production in wild-type *C. albicans* at 30 °C and 42 °C, in the presence
269 and absence of 4456dh. We observed that at 30 °C, there was a minimal amount of trehalose
270 detected and, therefore, there was no significant change detected in the presence of 4456dh (Fig.
271 5A). However, we observed a significant increase in trehalose content when *C. albicans* was

272 exposed to high temperature stress ($P < 0.0001$; Fig. 5A). The addition of 0.5 mM 4456dh to *C.*
273 *albicans* at 42 °C, resulted in an approximate two-fold decrease in trehalose content (Fig. 5A).
274 Similarly, we observed an increase in trehalose accumulation in *C. neoformans* cells grown at 37
275 °C, compared to 30 °C (Fig. 5B). Treatment of *C. neoformans* with a sublethal dose of 4456dh at
276 37 °C resulted in a significant decrease in trehalose ($P < 0.05$; Fig. 5B). Furthermore, this 4456dh-
277 mediated reduction in trehalose in *C. neoformans* occurred in a dose-dependent manner (Fig.
278 S10).

279 Tps1 is required for serum-induced filamentation in *C. albicans* and production of
280 polysaccharide capsule in *C. neoformans*, both of which are key virulence traits in these fungi
281 (23, 28, 40). Therefore, we investigated whether 4456dh-mediated inhibition of Tps1 results in
282 phenotypic recapitulation of a genetic deletion mutant lacking Tps1. Treatment of *C. albicans*
283 cells with 4456dh during hyphal-inducing conditions resulted in defective filamentation in a dose-
284 dependent manner with a complete inhibition of filamentation at sub-MIC concentration (5 μM)
285 (Fig. 5C). Similarly, capsule production was affected in *C. neoformans* upon 4456dh treatment in
286 a dose-dependent manner (Fig. 5D and S11). Combined, these assays directly show that
287 4456dh-mediated inhibition of Tps1 not only leads to less trehalose in fungal cells but also results
288 in phenotypes that are hallmarks of lack of functional Tps1 in these fungi. These data are
289 consistent with our hypothesis that 4456dh disrupts the substrate-binding capability of Tps1 and,
290 therefore, significantly lowers trehalose biosynthesis (Fig. 6).
291

292 **Discussion**

293 Fungal pathogens are devastating the ecosphere causing disease in agriculturally
294 important crops, amphibians, bats and humans. These invasive fungal infections are prevalent
295 worldwide and are responsible for millions of mortalities each year. To curb this significant rate of
296 disease and death, the development of the antifungal arsenal needs to be continued and
297 expanded to address concerns with antifungal drug resistance and the emergence of new fungal
298 pathogens due to many factors, including a warmer climate.

299 Here we have focused on the development of a lead compound that targets Tps1 from *C.*
300 *albicans* and *C. neoformans*, two predominant pathogenic fungal species in the clinics (1, 41).
301 They have been highlighted as critical pathogens by the World Health Organization (3). Tps1 is a
302 key enzyme in the critical first step of the trehalose biosynthesis pathway (15). Tps1 is a
303 glycosyltransferase enzyme that uses substrates UDPG and G6P to generate the intermediate,
304 trehalose-6-phosphate (T6P), which also acts as a signalling molecule. Tps1 is required for
305 growth at 37 °C, capsule formation and growth on glucose in *C. neoformans* and *C. gattii* (24, 25,
306 40). *C. albicans* Tps1 also contributes to pathogenesis-related factors such as biofilm formation
307 and hyphal transition from yeast (28). Perhaps most importantly, trehalose accumulates to high
308 levels upon exposure of *Candida* and *Cryptococcus* to heat stress (24, 25). Tps1 is required for
309 this response. Delineating this molecular mechanism and how to thwart it are critical to our
310 complete understanding of how these fungal pathogens can survive at the elevated body
311 temperature of the human host and cause disease.

312 4456dh is a soluble derivative of a lead compound identified in a screen to identify
313 inhibitors of CaTps1 catalytic activity. We determined, using orthogonal methods, including
314 microscale thermophoresis, thermal shift assays, a spectrophotometrically-coupled enzyme
315 assay and x-ray crystallography, that 4456dh binds and competitively inhibits the activity of Tps1
316 and 4456dh has bioactivity against a broad range of *Candida* and *Cryptococcus* species (Fig. 6).

317 Additionally, 4456dh also blocks the heat stress-induced hyperaccumulation of trehalose in both
318 *C. albicans* and *C. neoformans* (Fig. 5).

319 We also discovered that 4456dh may have an additional target. Given that it is a small
320 molecular weight compound, and GT-B glycosyltransferases have structurally conserved folds, it
321 is not surprising. We hypothesize that 4456dh may target another glycosyltransferase and predict
322 that it is one that does not involve a temperature-responsive phenotype because 4456dh retains
323 partial activity at 30 °C in a *C. deneoformans tps1*Δ mutant. We identified multiple proteins in *C.*
324 *albicans* and *C. neoformans* with structural similarity to Tps1 that may be affected by treatment
325 with 4456dh (Fig. S12 and Tables S2 - 4). Future work will be needed to identify and characterize
326 the additional target amongst these and other proteins.

327 There were great differences in the potency of 4456dh against fungal species. 4456dh
328 minimal inhibitory concentration values were the lowest for *C. glabrata*, reaching 7.8 μM, whilst
329 the other MICs were in the millimolar range for the fungi tested (Fig. 4). We were not able to find
330 a clear structural explanation for the differences, given the significant conservation of the residues
331 and structures of the substrate-binding pockets of Tps1 enzymes for these organisms (Fig. S5,6).
332 Therefore, we hypothesize that the ability of 4456dh to enter the cell may underly the range of
333 potency of 4456dh or the differences in the activity of 4456dh may also be due to the presence of
334 a secondary protein target amongst the *Candida* and *Cryptococcus*. In the future, we aim to
335 identify the additional target, or targets, of 4456dh using a directed, *in silico* approach to model
336 4456dh into glycosyltransferases in *Candida* and *Cryptococcus*. We shall also pursue a chemical
337 genomics approach to determine targets of 4456dh.

338 Whilst previous studies found that *C. neoformans tps1*Δ cells were less susceptible to
339 fluconazole at 30 °C, several studies have demonstrated that mutants in the trehalose
340 biosynthesis pathway enhance susceptibility to antifungal drugs at elevated temperatures (25, 39,
341 42). Given that a proposed role of trehalose is to stabilize membranes during stress, such as
342 elevated temperature, it is reasonable that loss of this protective sugar barrier would render the

343 cell membrane more susceptible to attack by polyenes, azoles and echinocandins. Future studies
344 will include investigations into the synergistic effects of 4456dh and the entire arsenal of the
345 current antifungal therapeutics in several *Candida* and *Cryptococcus* species under stress.

346 Additional future structure-activity relationship studies using 4456dh will benefit from our
347 initial structure of 4456dh bound to CaTps1. This scaffold, in addition to the previous structures
348 of Tps1 will direct more readily the generation of new derivatives of 4456dh into a more effective
349 Tps1-targeted drug. Our future studies will also include using medicinal chemistry to improve the
350 selectivity and bioactivity of 4456dh. Although the MIC values of 4456dh are not like those of
351 antifungals currently using in the clinic (Table S5), rational design of 4456dh analogues may
352 increase the likelihood of using a 4456 derivative as an antifungal therapeutic in clinics. We predict
353 that 4456dh analogues with increased specificity towards Tps1 will result in a compound with low
354 toxicity because the trehalose biosynthesis pathway is not found in mammals.

355 In this study, we have provided proof of principle for successful pharmacological inhibition
356 of Tps1, an enzyme in the trehalose biosynthesis pathway, which is central to fungal pathogen
357 virulence and thermotolerance.

358

359 **Methods and Materials**

360 **Strains**

361 Fungal strains used in this study are listed in Supplemental Table 5. Strains were stored as
362 glycerol stocks at -80 °C. Strains were grown at 30 °C on YPD (1% yeast extract, 2% Bacto
363 Peptone, 2% dextrose) agar plates.

364 **Fluorescence polarization screen**

365 The glycosyltransferase activity of 6xHis-CaTps1, which results in the release of UDP, was
366 measured using the UDP Transcreener Fluorescence Polarization (FP) assay (BellBrook Labs
367 #3018, Madison, WI). The St. Jude Children's Hospital (Memphis, TN) 3-point pharmacophore
368 (3PP) library was screened (36). Assays were performed at 37 °C for 60 minutes in a 384-well
369 plate using 5 μM 6xHis-CaTps1 in assay buffer containing 50 mM Tris-HCl pH 7.5, 300 mM NaCl,
370 10 mM $MgCl_2$ and 1 mM DTT. Fluorescence polarization was detected using a BMG Labtech
371 plate reader. Each assay plate contained the following additional control wells: (i) no antibody
372 control, (ii) DMSO vehicle control, (iii) novobiocin positive control and (iv) novobiocin dose-
373 response. Screens were performed by addition of single point additions of test molecules to the
374 above assay. The Z' factor was calculated according to guidelines by Zhang *et*. *al*., with a Z-factor
375 of 0.5 and 1.0 indicates an excellent assay (34).

376 ***De novo* co-crystallization and structure determination of *C. albicans* Tps1-4456 complex**

377 *C. albicans* Tps1 (6xHis-CaTps1) in SEC buffer (20 mM Tris-HCl pH 8.0, 200 mM NaCl, 5%
378 glycerol and 1 mM β-mercaptoethanol) was concentrated to 25 mg/mL using Amicon Ultra
379 concentrators (30 MWCO, Millipore). 4456 which was added to the crystallization drop to a final
380 concentration of 10 mM, from a 100 mM stock solution dissolved in 100% DMSO. Crystals were
381 grown at 25 °C by hanging-drop vapor diffusion methods. Diffraction-quality crystals appeared
382 after 3-4 days in a mother liquor solution containing 0.2 M magnesium sulfate, 0.1 M Tris-HCl pH
383 8.5 and 40% polyethylene glycol (PEG) 400. The crystals were cryo-preserved by looping and
384 dipping a crystal for 1-2 seconds in a solution containing the crystallization reagent supplemented

385 with 25% (v/v) glycerol. Data were collected at the Advanced Light Source (ALS) beamline 5.0.2
386 and processed with XDS (43). The structure of *C. albicans* Tps1-4456 was determined by
387 molecular replacement using the *C. albicans* Tps1-UDP-G6P complex (PDB 5HUU, (28)) as the
388 search model after removal of the UDP and G6P. Iterative cycles of model building were done in
389 COOT (44) and refinement using Phenix refine. Selected data collection and refinement statistics
390 are listed in Table 2.
391 Additional methodology for chemical synthesis, protein purification and several assays (binding,
392 activity, MIC, fungicidal, trehalose, zone of inhibition, filamentation, E-tests and capsule) can be
393 found in the Supplemental Material.
394

395 **Acknowledgements**

396 E.J.W is supported by the Duke Science and Technology Initiative. This work was also funded by
397 the grant NIH 1P01AI104533 to R.G.B., R.E.L., and J.R.P. J.R.P. is supported by grants AI73896
398 and A193257. V.Y. is supported by NIH/NIAID R01 awards AI039115-27 and AI172451-02
399 awarded to Joseph Heitman at Duke University Medical Center. C.B.N. is supported by grant
400 funding from the US NIH R01 AI175711.

401 We thank all current and past Washington and Brennan laboratory members for helpful
402 discussions. We are grateful to Dr. Joe Heitman for critical reading of the manuscript and Dr.
403 Andrew Alspaugh for thoughtful discussions on this project. We thank Dr. Angela Rivera, Natalie
404 Schulte and Dr. Peter Silinski for experimental support.

405 We thank the Advanced Light Source for access to 5.0.2. beamline. The Berkeley Center for
406 Structural Biology is supported by the Howard Hughes Medical Institute,
407 Participating Research Team members, and the National Institutes of Health, National Institute of
408 General Medical Sciences, ALS-ENABLE grant P30 GM124169. The Advanced Light Source is
409 a Department of Energy Office of Science User Facility under Contract No. DE-AC02-
410 05CH11231.

411 Y.M., V.Y., W.S. and E.J.W. conducted most experiments, and interpreted data and results. J.L.,
412 A.J., C.B.N., C.G., J.L.T. and M.S. conducted some experiments and interpreted data and results.
413 E.J.W. wrote the original draft of the manuscript. E.J.W., R.E.L., R.G.B and J.R.P. conceived the
414 study and interpreted data and results. E.J.W., V.Y., R.E.L., R.G.B and J.R.P. assisted with
415 editing the manuscript.

416 **Data Availability**

417 Atomic models of CaTps1-SJ6675 and CaTps1-4456 have been deposited in the RCSB Protein
418 Data Bank (PDB) (https://rcsb.org) with accession codes PDB ID 9NKB and PDB ID 9NIQ,
419 respectively. All additional data, including raw data and images associated with all figures, is
420 available upon reasonable request to R.G.B. and E.J.W., the corresponding authors.

421 **Figure Legends**

422 **Figure 1. Seven Tps1 inhibitors were identified using a high-throughput fluorescence**
423 **polarization screen. A)** Diagram of the Transcreener assay for Tps1 activity. **B)** Coomassie-
424 stained SDS polyacrylamide gel of purified recombinant 6xHis-CaTps1. Molecular weight markers
425 are shown with the 50 kDa protein standard highlighted with an arrow. **C)** Pipeline and results
426 from the Tps1 UDP Transcreener assay. **D)** Dot plot of % inhibition and compounds that were
427 tested for inhibition of 6xHis-CaTps1 activity. The 32 compounds above 10% inhibition at 500 μM
428 are highlighted. Highlighted in green are 6 of the compounds that resulted in dose-dependent
429 inhibition of 10% or greater of 6xHis-CaTps1 activity. In blue and highlighted with an arrow is
430 SJ6675. **E)** The chemical structures and identities of validated 6xHis-CaTps1-inhibiting hit
431 compounds. The compound SJ6675 used in additional studies is boxed.

432

433 **Figure 2. 4456dh binds Tps1 and inhibits Tps1 activity. A)** Structure of 4456dh. **B-C)** Glo-melt
434 thermal shift assays reveal 4456dh destabilizes 6xHis-CaTps1 (B) and 6xHis-CnTps1 (C). The
435 first derivative of the raw data was used to determine the melting temperature of 1 μM 6xHis-
436 CaTps1 (B) and 1 μM 6xHis-CnTps1 (C) treated without (black) or with 2 mM 4456dh (red). **D-E)**
437 Microscale thermophoresis assays demonstrate 4456dh binds to 6xHis-CaTps1 (D) and 6xHis-
438 CnTps1 (E) with indicated K_d. The top panel shows a representative of the MST trace with the
439 cold region labeled highlighted in blue and the hot region highlighted in red. The bottom panel
440 shows the dose-response curve. The resulting dose-response curves were fitted to a one-site
441 binding model to extract K_d values; the standard deviation was calculated using the K_d values
442 from each independent experiment (n=3). **F)** Tps1 enzyme activity assay with 5 μM 6xHis-CaTps1
443 (F) and 6xHis-CnTps1 (G) +/- 1 mM 4456dh. Error bars represent standard error. Comparison to
444 control, untreated 6xHis-CaTps1, was performed using Student's t-test; **$p < 0.01$, *** $p < 0.001$.

445

446 **Figure 3. Structure of *C. albicans* Tps1 in complex with 4456. A)** One subunit of the CaTps1-
447 4456 complex shown as a ribbon diagram. **B)** Surface-rendered structure revealing 4456, shown
448 as atomic-colored sticks, binds in the deep cavity of the substrate-binding pocket proximal to
449 known substrate-binding residues. **C)** Tps1 residues within 4 Å of 4456 are labelled, shown as
450 stick representations and indigo colored. **D)** Residues within 4 Å of 4456 are proximal to residues
451 that also interact with product and substrate, UDP and G6P (atom-colored sticks), in the CaTps1-
452 UDP-G6P complex (PDB: 5HUU) (28).
453
454 **Figure 4. 4456dh inhibits the growth of *Candida* and *Cryptococcus* species.** Two-fold dose
455 response assays were performed against **A)** *C. albicans* at 42 °C and *C. auris* at 39 °C, **B)** *C.*
456 *glabrata* at 42 °C, and **C)** *C. neoformans*, *C. deneoformans* and *C. gattii* at 37 °C. 4456dh was
457 administered at the concentrations indicated. Cultures were grown in YPD at the listed
458 temperatures for 48 hours for *Candida* species and 72 hours for *Cryptococcus* species.
459 Experimental temperatures reflect the temperatures at which the fungi experience heat stress.
460 (Left) Relative growth of treated samples was calculated by averaging technical triplicates and
461 normalizing the OD_{600} of each treated well to the average OD_{600} of the untreated wild-type
462 controls, after the absorbance due to the compound was subtracted. The MIC_{80} values, calculated
463 based on the OD_{600} values, are indicated in the white text on each heat map. (Right)
464 Representative spot assays show the ability of cells to grow after exposure to 4456dh and indicate
465 fungicidal activity of 4456dh.
466
467 **Figure 5. 4456dh treatment results in reduced trehalose accumulation and a decrease in**
468 **Tps1-dependent virulence factors.** Trehalose accumulation measurements for *C. albicans* **(A)**
469 and *C. neoformans* **(B)** cultured at indicated temperatures in the absence or presence of 0.5 mM
470 4456dh. Trehalose was measured using a colorimetric glucose assay after treatment of cultures
471 with trehalase. Statistical comparisons were done with a one-way ANOVA analysis followed by a

472 posthoc Tukey's test. Error bars represent standard error. **C)** *C. albicans* wild-type strain SC5314
473 cells were treated with 0.5 mM, 1.0 mM and 5 mM 4456dh. Untreated *C. albicans* WT cells and
474 the *C. albicans tps1*Δ/*tps1*Δ deletion strain were included in this experiment as positive and
475 negative controls, respectively. Increasing concentrations of 4456dh negatively affect
476 filamentation in *C. albicans* in YPD plus 10% fetal bovine serum incubated at 37 °C for 2 hours.
477 Representative images from 2 independent experiments are shown. The scale bars represent 10
478 microns. **D)** Analysis of capsule formation in C. neoformans wild-type H99 using India Ink counter-
479 staining in cells treated with 0.1, 0.5 mM and 1 mM 4456dh. Untreated *C. neoformans* WT cells
480 and the *C. neoformans tps1*Δ deletion strain were included in this experiment as positive and
481 negative controls, respectively. The cells were grown for 72 hours at 30 °C in capsule-inducing
482 conditions. Cells were harvested, stained in India Ink and analyzed using differential interference
483 contrast (DIC) imaging. Representative images from 3 independent experiments are shown.
484 Scale bar represents 10 microns.
485
486 **Figure 6. Model for 4456dh activity in fungal cells.** Trehalose biosynthesis in *Cryptococcus*
487 and *Candida* is initiated by Tps1, which converts G6P and UDPG into trehalose-6-phosphate
488 (T6P). In the second step of the trehalose biosynthesis pathway, T6P is dephosphorylated by
489 Tps2 and trehalose is generated. As shown, Tps1 from *C. neoformans* forms a homotetramer
490 (30). 4456dh binds the exposed substrate-binding pockets of Tps1. Additionally, 4456dh may
491 have an additional target that is likely another glycosyltransferase in some fungal organisms.
492
493

494 **Tables**

495 **Table 1. Small molecules identified in high-throughput screen that inhibit the activity of**
496 **6xHis-CaTps1.**

497

Compound	Chemical Formula	Molecular Weight	CaTps1 FP (% inhibition)	CaTps1 Inhibition Assay (μM)
SJ000805629-1	$C_7H_5NO_2$	135.12	32.19	685.4
SJ000866675-1	$C_7H_6N_2OS$	166.20	13.69	983.3
SJ000866077-1	$C_8H_{13}NO_3S$	203.26	11.12	1231.5
SJ000866063-1	$C_{10}H_{11}ClN_2$	194.66	18.96	767.5
SJ000866107-1	$C_{11}H_{13}ClN_2$	208.69	18.24	1152.3
SJ000866390-1	$C_{10}H_{13}N_3$	175.24	36.36	608.7
SJ000866536-1	$C_9H_{16}N_2O$	168.24	18.64	546.9

498

499

500 **Table 2. Data collection and refinement statistics of structure of 6xHis-CaTps1 in**
501 **complex with 4456.**
502

6xHisCaTps1 – 4456 complex	
Resolution range	58.78 - 3.35 (3.47 - 3.35)
Space group	P 6_4 2 2
Unit cell	117.6 117.6 134.0 90 90 120
Total reflections	75,865 (7,778)
Unique reflections	7,644 (753)
Multiplicity	9.9 (10.3)
Completeness (%)	91.66 (94.0)
Mean I/sigma(I)	14.9 (3.3)
Wilson B-factor	78.7
R-merge	0.1037 (0.2833)
R-meas	0.1089 (0.297)
R-pim	0.03209 (0.08654)
$CC_{1/2}$	0.998 (0.932)
CC*	0.999 (0.982)
Reflections used in refinement	7641 (753)
Reflections used for R-free	716 (71)
R-work	0.2504 (0.3147)
R-free	0.2893 (0.3509)
Number of non-hydrogen atoms	3644
macromolecules	3623
ligands	21
solvent	0
Protein residues	456
RMS(bonds)	0.003
RMS(angles)	0.53
Ramachandran favored (%)	94.9
Ramachandran allowed (%)	4.45
Ramachandran outliers (%)	0.67
Rotamer outliers (%)	0.00
Clashscore	5.12
Average B-factor	83.35
macromolecules	83.25
ligands	100.62

503 Statistics for the highest-resolution shell are shown in parentheses.
504

505 **References**

506 1. Brown GD, Denning DW, Gow NAR, Levitz SM, Netea MG, White TC. 2012. Hidden killers:
507 human fungal infections. Sci Transl Med 4:165rv13.

508 2. Denning DW. 2024. Global incidence and mortality of severe fungal disease. Lancet Infect
509 Dis S1473-3099(23)00692–8.

510 3. 2022. WHO Fungal Priority Pathogens List to Guide Research, Development and Public
511 Health Action. World Health Organization, Geneva.

512 4. Puumala E, Fallah S, Robbins N, Cowen LE. 2024. Advancements and challenges in
513 antifungal therapeutic development. Clin Microbiol Rev 37:e0014223.

514 5. May RC, Stone NRH, Wiesner DL, Bicanic T, Nielsen K. 2016. *Cryptococcus*: from
515 environmental saprophyte to global pathogen. Nature Reviews Microbiology 14:106–117.

516 6. Nnadi NE, Carter DA. 2021. Climate change and the emergence of fungal pathogens. PLoS
517 Pathog 17:e1009503.

518 7. Garcia-Solache MA, Casadevall A. 2010. Global warming will bring new fungal diseases for
519 mammals. mBio 1:e00061-10.

520 8. Casadevall A. 2020. Climate change brings the specter of new infectious diseases. J Clin
521 Invest 130:553–555.

522 9. Casadevall A, Kontoyiannis DP, Robert V. 2019. On the Emergence of *Candida auris*:
523 Climate Change, Azoles, Swamps, and Birds. mBio 10.

524 10. Chaabane F, Graf A, Jequier L, Coste AT. 2019. Review on Antifungal Resistance
525 Mechanisms in the Emerging Pathogen *Candida auris*. Frontiers in Microbiology 10:2788.

526 11. Casadevall A, Kontoyiannis DP, Robert V. 2021. Environmental *Candida auris* and the
527 Global Warming Emergence Hypothesis. mBio 12:e00360-21.

528 12. Perfect JR, Tenor JL, Miao Y, Brennan RG. 2017. Trehalose pathway as an antifungal target.
529 Virulence 8:143–149.

530 13. Gancedo C, Flores C-L. 2004. The importance of a functional trehalose biosynthetic pathway
531 for the life of yeasts and fungi. FEMS Yeast Res 4:351–359.

532 14. Kern C, Wolf C, Bender F, Berger M, Noack S, Schmalz S, Ilg T. 2012. Trehalose-6-
533 phosphate synthase from the cat flea *Ctenocephalides felis* and *Drosophila melanogaster*:
534 gene identification, cloning, heterologous functional expression and identification of
535 inhibitors by high throughput screening. Insect Mol Biol 21:456–471.

536 15. Thammahong A, Puttikamonkul S, Perfect JR, Brennan RG, Cramer RA. 2017. Central Role
537 of the Trehalose Biosynthesis Pathway in the Pathogenesis of Human Fungal Infections:
538 Opportunities and Challenges for Therapeutic Development. Microbiol Mol Biol Rev 81.

539 16. Al-Bader N, Vanier G, Liu H, Gravelat FN, Urb M, Hoareau CM-Q, Campoli P, Chabot J,
540 Filler SG, Sheppard DC. 2010. Role of trehalose biosynthesis in *Aspergillus fumigatus*
541 development, stress response, and virulence. Infect Immun 78:3007–3018.

542 17. Bell W, Sun W, Hohmann S, Wera S, Reinders A, De Virgilio C, Wiemken A, Thevelein JM.
543 1998. Composition and functional analysis of the *Saccharomyces cerevisiae* trehalose
544 synthase complex. J Biol Chem 273:33311–33319.

545 18. Elliott B, Haltiwanger RS, Futcher B. 1996. Synergy between trehalose and Hsp104 for
546 thermotolerance in *Saccharomyces cerevisiae*. Genetics 144:923–933.

547 19. Singer MA, Lindquist S. 1998. Thermotolerance in *Saccharomyces cerevisiae*: the Yin and
548 Yang of trehalose. Trends Biotechnol 16:460–468.

549 20. Tapia H, Young L, Fox D, Bertozzi CR, Koshland D. 2015. Increasing intracellular trehalose
550 is sufficient to confer desiccation tolerance to *Saccharomyces cerevisiae*. Proc Natl Acad
551 Sci U S A 112:6122–6127.

552 21. Meikle AJ, Chudek JA, Reed RH, Gadd GM. 1991. Natural abundance 13C-nuclear
553 magnetic resonance spectroscopic analysis of acyclic polyol and trehalose accumulation by
554 several yeast species in response to salt stress. FEMS Microbiol Lett 66:163–167.

555 22. Crowe JH, Crowe LM, Chapman D. 1984. Preservation of membranes in anhydrobiotic
556 organisms: the role of trehalose. Science 223:701–703.

557 23. Zaragoza O, Blazquez MA, Gancedo C. 1998. Disruption of the *Candida albicans* TPS1
558 gene encoding trehalose-6-phosphate synthase impairs formation of hyphae and decreases
559 infectivity. J Bacteriol 180:3809–3815.

560 24. Ngamskulrungroj P, Himmelreich U, Breger JA, Wilson C, Chayakulkeeree M,
561 Krockenberger MB, Malik R, Daniel H-M, Toffaletti D, Djordjevic JT, Mylonakis E, Meyer W,
562 Perfect JR. 2009. The trehalose synthesis pathway is an integral part of the virulence
563 composite for *Cryptococcus gattii*. Infect Immun 77:4584–4596.

564 25. Petzold EW, Himmelreich U, Mylonakis E, Rude T, Toffaletti D, Cox GM, Miller JL, Perfect
565 JR. 2006. Characterization and regulation of the trehalose synthesis pathway and its
566 importance in the pathogenicity of *Cryptococcus neoformans*. Infect Immun 74:5877–5887.

567 26. Martínez-Esparza M, Martínez-Vicente E, González-Párraga P, Ros JM, García-Peñarrubia
568 P, Argüelles J-C. 2009. Role of trehalose-6P phosphatase (TPS2) in stress tolerance and
569 resistance to macrophage killing in *Candida albicans*. Int J Med Microbiol 299:453–464.

570 27. Van Dijck P, De Rop L, Szlufcik K, Van Ael E, Thevelein JM. 2002. Disruption of the *Candida*
571 *albicans* TPS2 gene encoding trehalose-6-phosphate phosphatase decreases infectivity
572 without affecting hypha formation. Infect Immun 70:1772–1782.

573 28. Miao Y, Tenor JL, Toffaletti DL, Maskarinec SA, Liu J, Lee RE, Perfect JR, Brennan RG.
574 2017. Structural and In Vivo Studies on Trehalose-6-Phosphate Synthase from Pathogenic
575 Fungi Provide Insights into Its Catalytic Mechanism, Biological Necessity, and Potential for
576 Novel Antifungal Drug Design. mBio 8.

577 29. Miao Y, Tenor JL, Toffaletti DL, Washington EJ, Liu J, Shadrick WR, Schumacher MA, Lee
578 RE, Perfect JR, Brennan RG. 2016. Structures of trehalose-6-phosphate phosphatase from
579 pathogenic fungi reveal the mechanisms of substrate recognition and catalysis. Proc Natl
580 Acad Sci U S A 113:7148–7153.

581 30. Washington EJ, Zhou Y, Hsu AL, Petrovich M, Tenor JL, Toffaletti DL, Guan Z, Perfect JR,
582 Borgnia MJ, Bartesaghi A, Brennan RG. 2024. Structures of trehalose-6-phosphate
583 synthase, Tps1, from the fungal pathogen *Cryptococcus neoformans*: A target for
584 antifungals. Proc Natl Acad Sci U S A 121:e2314087121.

585 31. Breton C, Snajdrová L, Jeanneau C, Koca J, Imberty A. 2006. Structures and mechanisms
586 of glycosyltransferases. Glycobiology 16:29R-37R.

587 32. Owicki JC. 2000. Fluorescence Polarization and Anisotropy in High Throughput Screening:
588 Perspectives and Primer. Journal of Biomolecular Screening 5:297–306.

589 33. Lowery RG, Kleman-Leyer K. 2006. Transcreener™: screening enzymes involved in
590 covalent regulation. Expert Opinion on Therapeutic Targets 10:179–190.

591 34. Zhang JH, Chung TD, Oldenburg KR. 1999. A Simple Statistical Parameter for Use in
592 Evaluation and Validation of High Throughput Screening Assays. J Biomol Screen 4:67–73.

593 35. Pan YT, Elbein AD. 1996. Inhibition of the trehalose-P synthase of mycobacteria by various
594 antibiotics. Arch Biochem Biophys 335:258–266.

595 36. Nishiguchi G, Das S, Ochoada J, Long H, Lee RE, Rankovic Z, Shelat AA. 2021. Evaluating
596 and evolving a screening library in academia: the St Jude approach. Drug Discov Today
597 26:1060–1069.

598 37. Liebschner D, Afonine PV, Moriarty NW, Poon BK, Sobolev OV, Terwilliger TC, Adams PD.
599 2017. Polder maps: improving OMIT maps by excluding bulk solvent. Acta Crystallographica
600 Section D 73:148–157.

601 38. Glaser F, Pupko T, Paz I, Bell RE, Bechor-Shental D, Martz E, Ben-Tal N. 2003. ConSurf:
602 identification of functional regions in proteins by surface-mapping of phylogenetic
603 information. Bioinformatics 19:163–164.

604 39. Zhu Q, Wijnants S, Feil R, Genechten WV, Vergauwen R, Goethem OV, Lunn JE, Ende MV,
605 Dijck PV. 2025. The stress-protectant molecule trehalose mediates fluconazole tolerance in
606 *Candida glabrata*. Antimicrobial Agents and Chemotherapy 69:e01349-24.

607 40. Goughenour K, Creech A, Xu J, He X, Hissong R, Giamberardino C, Tenor J, Toffaletti D,
608 Perfect J, Olszewski M. 2024. *Cryptococcus neoformans* trehalose-6-phosphate synthase
609 (tps1) promotes organ-specific virulence and fungal protection against multiple lines of host
610 defenses. Front Cell Infect Microbiol 14:1392015.

611 41. Fisher MC. 2012. Emerging fungal threats to animal, plant and ecosystem health. Nature
612 484.

613 42. Guirao-Abad JP, Pujante V, Sánchez-Fresneda R, Yagüe G, Argüelles J-C. 2019. Sensitivity
614 of the *Candida albicans* trehalose-deficient mutants *tps1*Δ and *tps2*Δ to amphotericin B and
615 micafungin. J Med Microbiol 68:1479–1488.

616 43. Kabsch W. 2010. XDS. Acta Crystallogr D Biol Crystallogr 66:125–132.

617 44. Emsley P, Cowtan K. 2004. Coot: model-building tools for molecular graphics. Acta
618 Crystallogr D Biol Crystallogr 60:2126–2132.

619

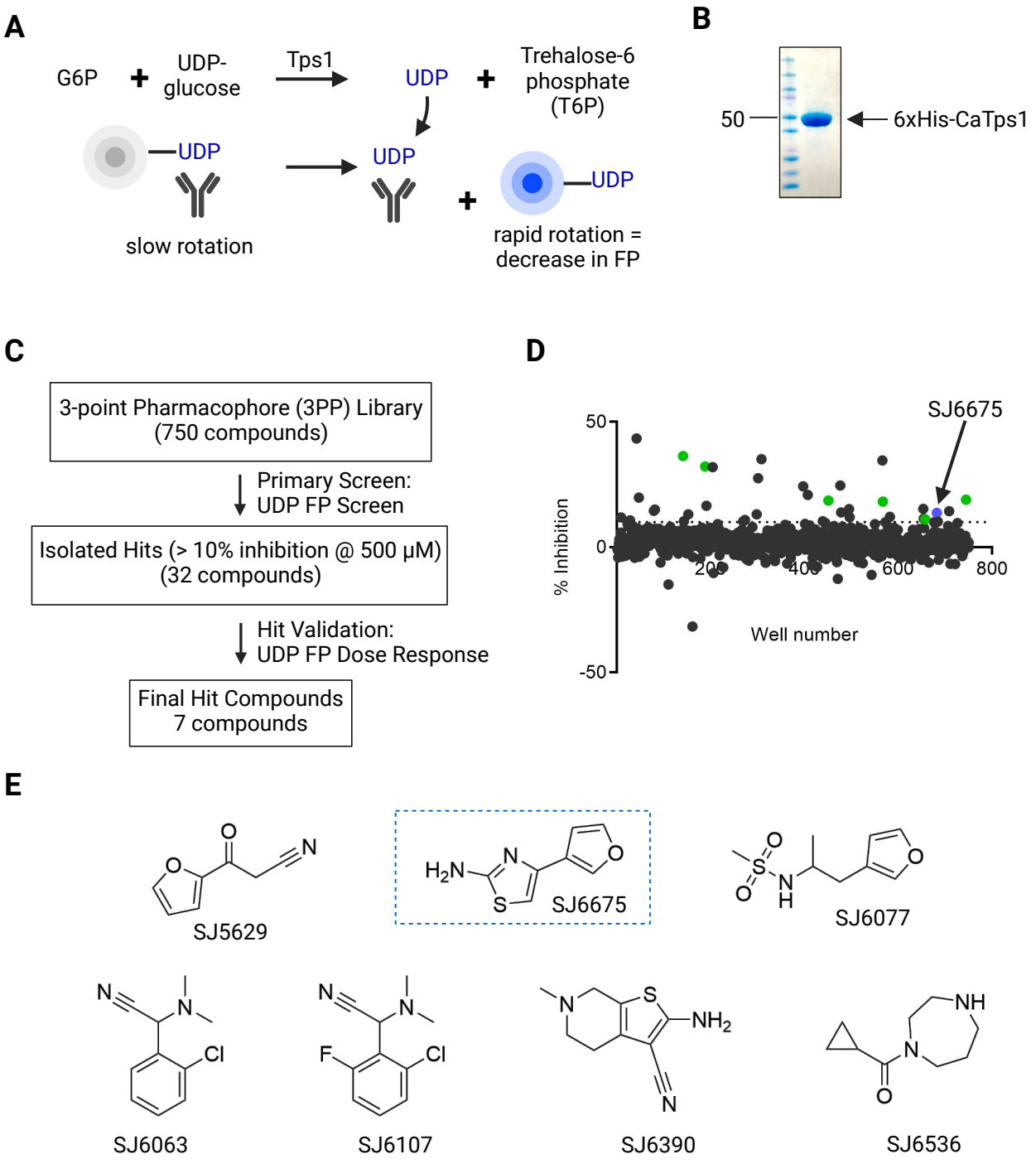
A
G6P
UDP-glucose
Tps1
UDP
Trehalose-6 phosphate (T6P)
UDP
UDP
UDP
slow rotation
rapid rotation = decrease in FP
B
50
6xHis-CaTps1
C
3-point Pharmacophore (3PP) Library (750 compounds)
Primary Screen: UDP FP Screen
Isolated Hits (> 10% inhibition @ 500 μM) (32 compounds)
Hit Validation: UDP FP Dose Response
Final Hit Compounds 7 compounds
D
SJ6675
50
0
-50
% Inhibition
200
400
600
800
Well number
E
SJ5629
SJ6675
SJ6077
SJ6063
SJ6107
SJ6390
SJ6536

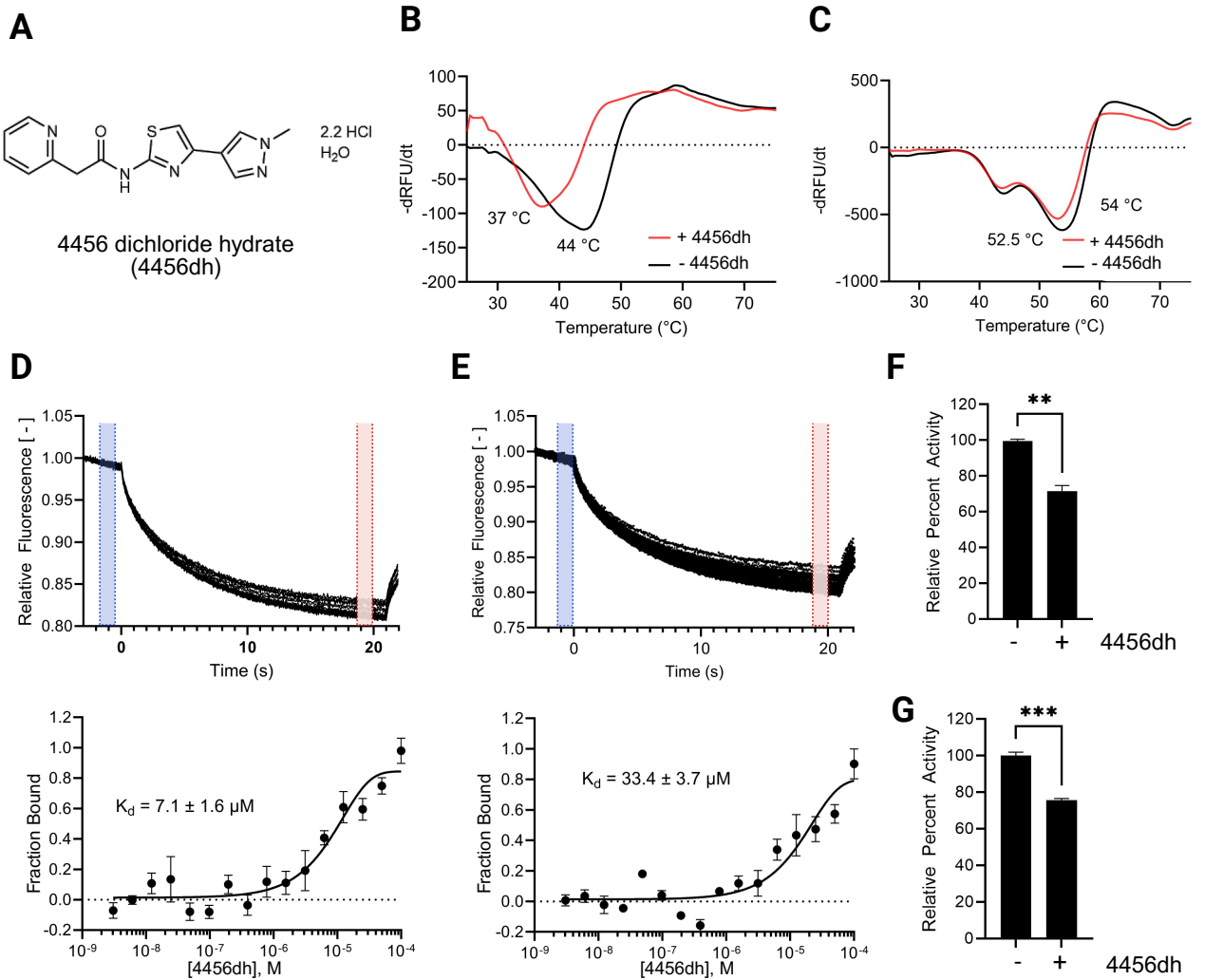
A
2.2 HCl
H2O
4456 dichloride hydrate
(4456dh)
B
-dRFU/dt
37 °C
44 °C
+ 4456dh
- 4456dh
Temperature (°C)
C
-dRFU/dt
54 °C
52.5 °C
+ 4456dh
- 4456dh
Temperature (°C)
D
Relative Fluorescence [-]
Time (s)
Fraction Bound
Kd = 7.1 ± 1.6 μM
[4456dh], M
E
Relative Fluorescence [-]
Time (s)
Fraction Bound
Kd = 33.4 ± 3.7 μM
[4456dh], M
F
Relative Percent Activity
**
- + 4456dh
G
Relative Percent Activity
***
- + 4456dh

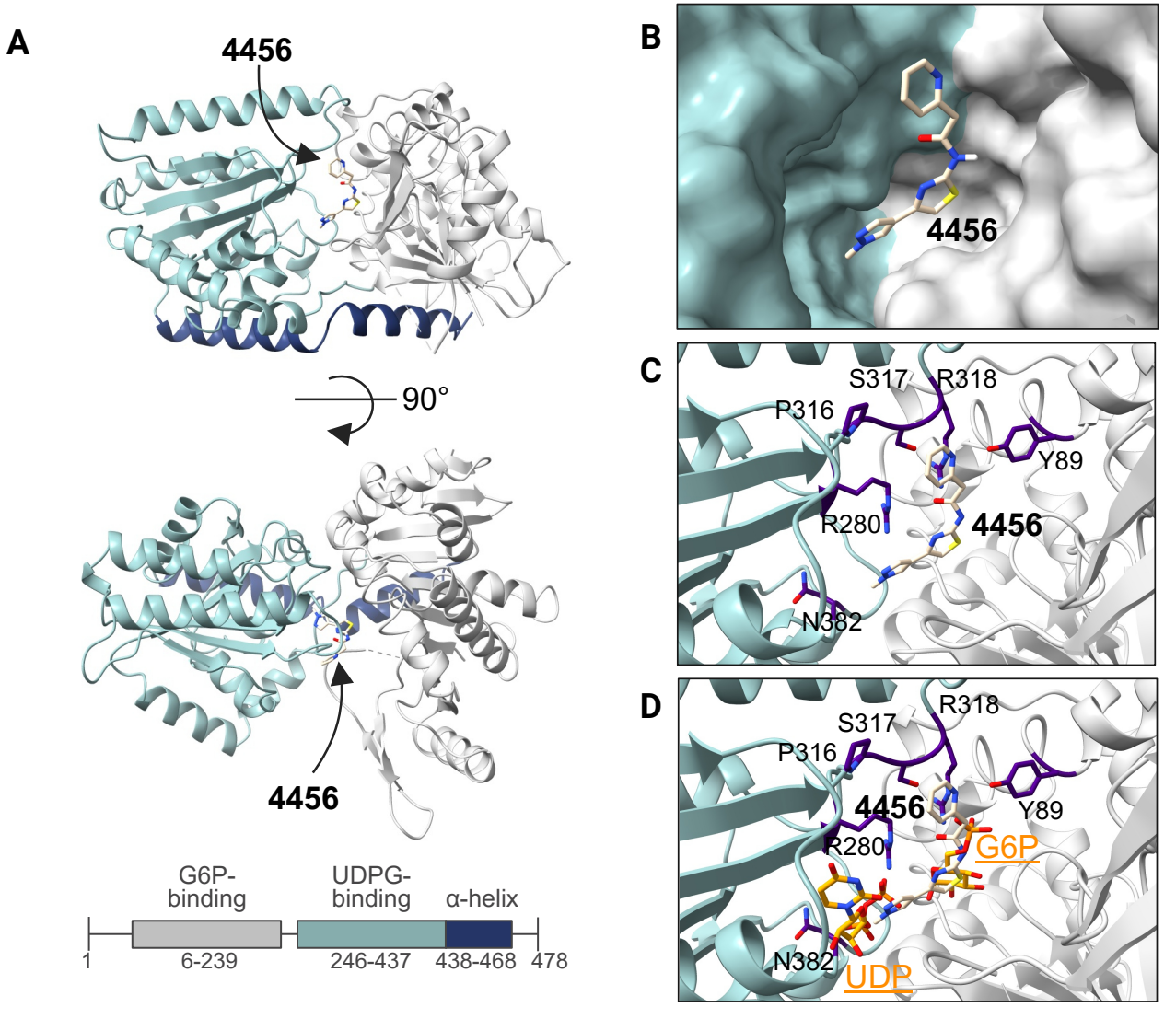
A
4456
90°
4456
G6P-
binding
UDPG-
binding
α-helix
1
6-239
246-437
438-468
478
B
4456
C
S317
R318
P316
Y89
R280
4456
N382
D
R318
S317
P316
4456
Y89
R280
G6P
N382
UDP

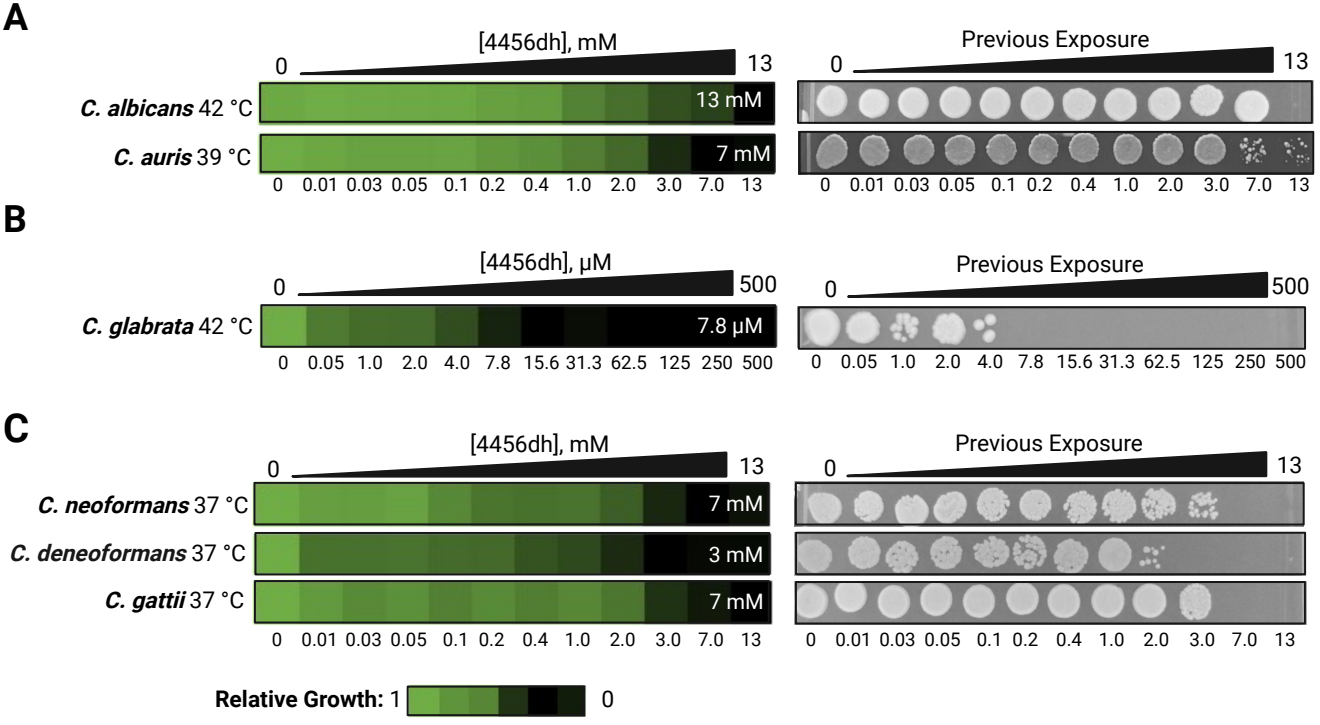
A
[4456dh], mM
0
13
Previous Exposure
0
13
C. albicans 42 °C
13 mM
C. auris 39 °C
7 mM
0 0.01 0.03 0.05 0.1 0.2 0.4 1.0 2.0 3.0 7.0 13
0 0.01 0.03 0.05 0.1 0.2 0.4 1.0 2.0 3.0 7.0 13
B
[4456dh], µM
0
500
Previous Exposure
0
500
C. glabrata 42 °C
7.8 µM
0 0.05 1.0 2.0 4.0 7.8 15.6 31.3 62.5 125 250 500
0 0.05 1.0 2.0 4.0 7.8 15.6 31.3 62.5 125 250 500
C
[4456dh], mM
0
13
Previous Exposure
0
13
C. neoformans 37 °C
7 mM
C. deneoformans 37 °C
3 mM
C. gattii 37 °C
7 mM
0 0.01 0.03 0.05 0.1 0.2 0.4 1.0 2.0 3.0 7.0 13
0 0.01 0.03 0.05 0.1 0.2 0.4 1.0 2.0 3.0 7.0 13
Relative Growth: 1
0

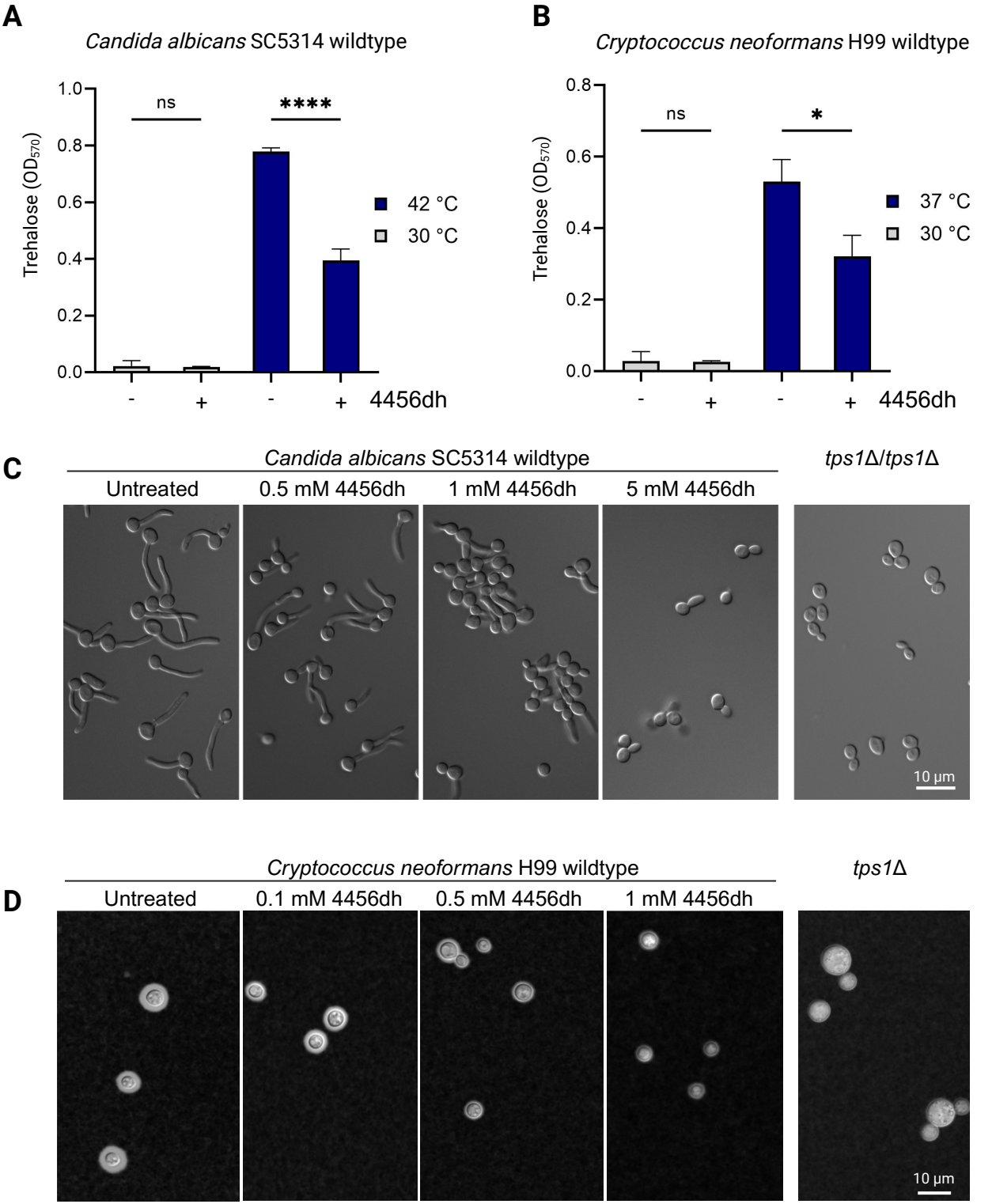
A
Candida albicans SC5314 wildtype
Trehalose (OD570)
1.0
0.8
0.6
0.4
0.2
0.0
ns
****
42 °C
30 °C
-
+
-
+
4456dh
B
Cryptococcus neoformans H99 wildtype
Trehalose (OD570)
0.8
0.6
0.4
0.2
0.0
ns
*
37 °C
30 °C
-
+
-
+
4456dh
C
Candida albicans SC5314 wildtype
tps1Δ/tps1Δ
Untreated
0.5 mM 4456dh
1 mM 4456dh
5 mM 4456dh
10 µm
D
Cryptococcus neoformans H99 wildtype
tps1Δ
Untreated
0.1 mM 4456dh
0.5 mM 4456dh
1 mM 4456dh
10 µm

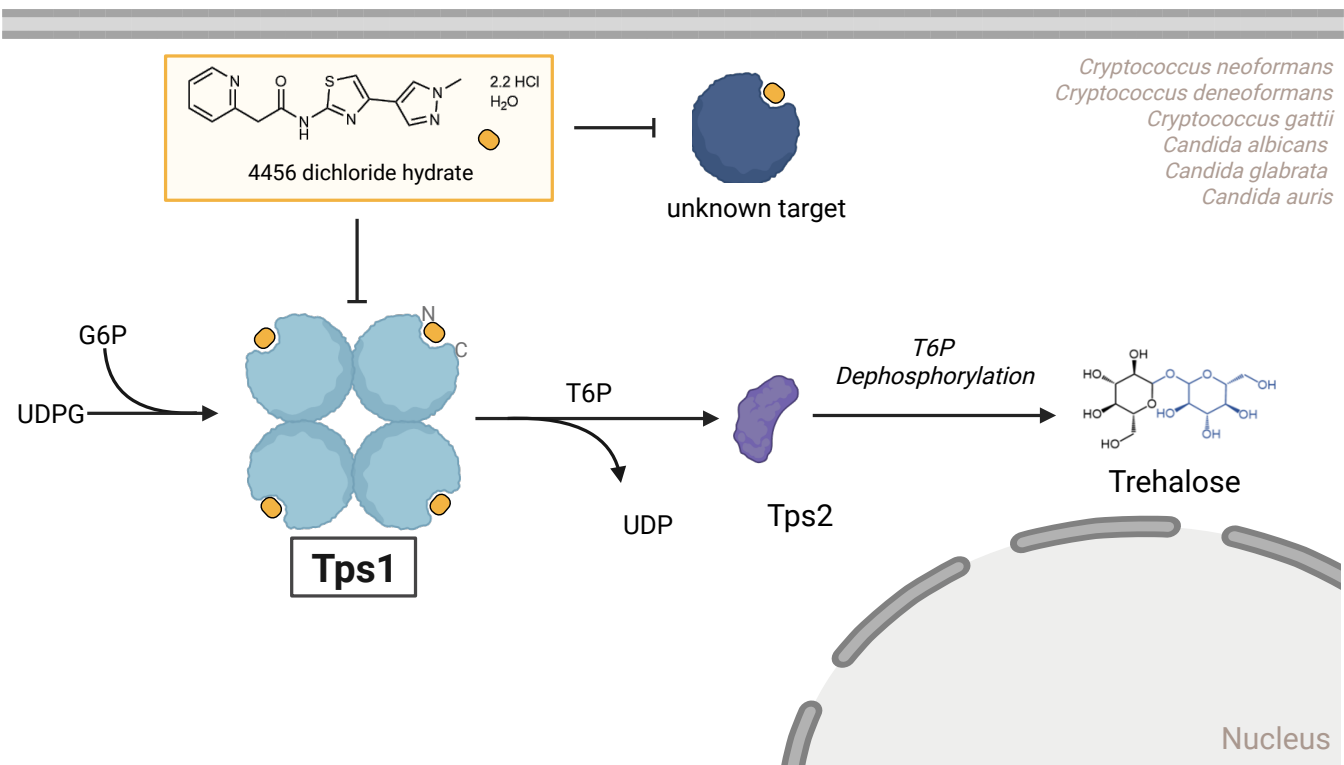
4456 dichloride hydrate
2.2 HCl
H_2O
unknown target
Cryptococcus neoformans
Cryptococcus deneoformans
Cryptococcus gattii
Candida albicans
Candida glabrata
Candida auris
G6P
UDPG
N
C
Tps1
T6P
UDP
Tps2
T6P
Dephosphorylation
Trehalose
Nucleus